IEEE Access
Multidisciplinary ⋮ Rapid Review ⋮ Open Access Journal

Received 17 February 2023, accepted 2 March 2023, date of publication 8 March 2023, date of current version 15 March 2023.

Digital Object Identifier 10.1109/ACCESS.2023.3254299

RESEARCH ARTICLE

Reduced Reference Frame Transformation Assessment in Unbalanced Three-Phase Four-Wire Systems

FRANCISCO CASADO-MACHADO, JOSÉ L. MARTÍNEZ-RAMOS, (Senior Member, IEEE), MANUEL BARRAGÁN-VILLAREJO, AND JOSÉ MARÍA MAZA-ORTEGA, (Member, IEEE)
Department of Electrical Engineering, University of Seville, 41092 Seville, Spain

Corresponding author: Francisco Casado-Machado (mfrancisco@us.es)

This work was supported in part by the Ministerio de Ciencia e Innovación (MCIN) /Agencia Estatal de Investigación (AEI)/ 10.13039/501100011033 through the "European Regional Development Fund (ERDF) A way of making Europe" under Grant PID2021-124571OB-I00; and in part by the CERVERA Research Program of Centro para el Desarrollo Tecnológico y la Innovación (CDTI), Industrial and Technological Development Centre of Spain, through the Project HySGrid+ under Grant CER-20191019.

ABSTRACT Three-phase four-wire systems require a reference frame similar to that used in 3-phase 3-wire system configurations that allow them to be easily analysed, modelled and controlled. A new reference frame called Reduced Reference Frame (RRF) was presented by the authors in a previous work to satisfy these objectives. This is based on the locus of the voltage space vector which is used to perform a transformation applied to 3-phase 4-wire systems. This paper uses the proposed RRF to demonstrate the benefits of this transformation under different conditions of load or voltage imbalance. To this end, the different types of imbalances considered are studied by comparing the results in the classical $\alpha\beta\gamma$ axes, the so-called *mno*-transform specifically developed for 3-phase 4-wire systems and the RRF coordinates. In addition, a theoretical identification of some types of imbalances is done comparing the simulation results and the fundamentals of the RRF.

INDEX TERMS Coordinate transformation, reference frame, three–phase four–wire system, unbalanced power system.

I. INTRODUCTION

The integration of distributed energy resources such as photovoltaic plants, energy storage systems, or electric vehicles in low-voltage networks will require more detailed studies of three-phase four-wire systems. These will be deployed in a three-phase or single-phase manner depending on the power to be managed by each resource, which could lead to a greater imbalance of these networks. An example of this situation can be found in [1], where a year-long campaign was carried out to measure the currents and voltages on the low-voltage side of more than a hundred transformers integrated in a network with high PV penetration in Great Britain. The report shows an average voltage imbalance in the transformers of more than 0.5%, with some of them reaching maximum imbalances of more than 5% in certain moments. In this situation, the neutral wire current may be high with maximum values above the rated current during some periods. In addition, in electrical systems such as microgrids, it is common to find load and generation imbalance conditions, due to the single-phase character of the consumers/generators and to the different demand/generation of each of them [2], [3]. This situation becomes more pronounced for islanded microgrids dominated by power converters, where it is especially interesting to have the ability to control the voltage and currents of these power converters in an unbalance way [2], [3]. This way, it could be possible to improve the general performance of the microgrid [4].

As a consequence, it is essential to define an adequate reference frame that allows to analyze, model, and control three-phase four-wire systems with a high level of imbalance.

The classical reference frames based on the Clarke et al. [5] and Park [6] transforms have proven to be successful in three-phase three-wire systems. However, for three-phase four-wire

The associate editor coordinating the review of this manuscript and approving it for publication was Yizhang Jiang.

systems, a more general approach than the one proposed by Akagi et al. in [7] is required for a better understanding of how the unbalanced magnitudes may affect the active and reactive instantaneous powers [8]. In recent years, several transformations have emerged to address this issue. Of special interest are those based on Singular Value Decomposition proposed by V. Choqueuse in [9] or those based on the Frenet-Serret frame proposed by Granjon and Phua [10] and more recently Milano et al. [11]. Others authors use tensor algebra [12], while others apply the geometric or Clifford algebra to analyze three-phase four wire systems [13], [14] or multiphase power systems in time-domain [15], [16].

Other authors apply transformation methods based on the voltage space vector and its time derivative to define a stationary *mno* reference frame, whose orientation depends on the system imbalance [17]. In addition, the active and reactive power terms can be related to the corresponding voltages and currents in the *mno* reference frame. Nevertheless, this frame is undefined for some particular voltage conditions, i.e. a voltage with just zero-sequence component or null voltage in the phase *a* [17]. A similar approach was proposed by Tan et al. [18], representing unbalanced signals in a non-orthogonal reference frame by means of a space vector for 3-phase 3-wire systems. This strategy was recently extended for 3-phase 4-wire systems in [19] and [20]. Despite the extension of the transform, it is not defined if any of the phase magnitudes of the system is null or the phase difference between two of them is 0 or π radians [21].

To cover all possible imbalances within 3-phase 4-wires systems, the authors recently presented a new reference frame called Reduced Reference Frame (RRF) [22] whose orientation depends on the trajectory, or locus, defined by the space vector of the analysed three–phase *abc* magnitude. This allows to formulate a power theory for computing the instantaneous active and reactive power similar to the one proposed by Akagi et al. for three-phase balanced systems in [7]. Additionally, the axes that define these coordinates are oriented taking advantage of the locus geometry. Specifically, they are oriented on the semi-major and semi-minor axes of its geometry. This brings a series of benefits once the space vector of the measured signals are expressed in terms of the RRF: (i) a dimensional reduction of the space vector from three to two coordinates and (ii) both coordinates are sinusiodal signals delayed a quarter of cycle and their amplitudes are related through the locus eccentricity. Moreover, this locus eccentricity allows to compute one RRF magnitude from the other one. In addition, this parameter can be used to classify the imbalances of 3-phase 4-wire systems depending on the locus shape.

The RRF advantages have been also addressed in dynamic scenarios and protection systems. Particularly, the dynamics of the space vectors related to first-order 3-phase 4-wire circuits with different imbalances has been analyzed in [23]. Its application for line protection has been reported in [24]. This time-domain protection technique detects the fault type based on the variation of the angle between the space vectors related to voltages and currents.

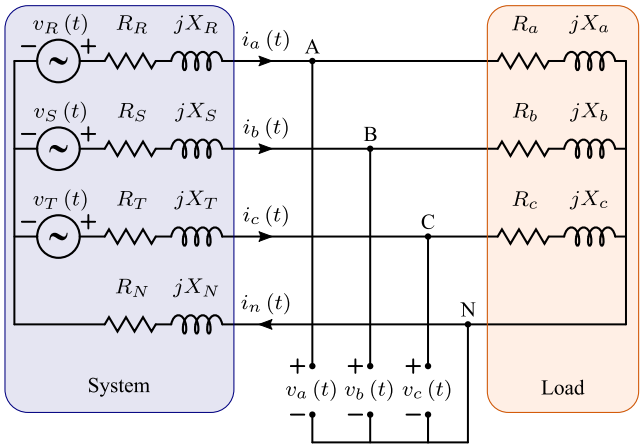

FIGURE 1. Three–phase four–wire system under study.

The objective of this paper is to show and to interpret several case studies of unbalanced 3-phase 4-wires systems using the RRF proposed by the authors in [22]. For this purpose, a three-phase four-wire circuit composed of three voltage sources feeding a three-phase load is analysed working under load and voltage imbalances. The voltage and current in the load will be transformed using the classical Clarke transform, the *mno* axes and the recently proposed RRF coordinates. This will allow to demonstrate the benefits of the RRF approach compared to the Clarke and *mno* transformations in terms of unbalance classification, computation of the power terms and the relationships between the transformed magnitudes.

The paper is organized as follows: Section II presents the most relevant concepts of the RRF transform. Section III presents several case studies for evaluating the performance of the RRF under unbalanced voltages and loads. Finally, Section IV presents the most important conclusions of this work.

II. REDUCED REFERENCE FRAME TRANSFORMATION

The theoretical fundamentals and mathematical formulation of the RRF transformation are fully described in [22]. This section presents the most important concepts on which the RRF transform is based to understand the results presented throughout the paper.

Let us consider a three-phase four-wire system as shown in Fig. 1, where up to three linear independent line voltages $v_a(t)$, $v_b(t)$ and $v_c(t)$ can be defined taking the voltage of the fourth wire as the voltage reference. Expressing the generic set of the linearly independent line voltages as:

$$v_{ph}(t) = \sqrt{2}\, V_{ph} \cos\left(\omega t + \theta_{ph}\right) \quad ph = a, b, c, \qquad (1)$$

where ph is the tag of the wire, ω is the angular frequency, V_{ph} and θ_{ph} are the RMS value and phase angle of the voltage respectively.

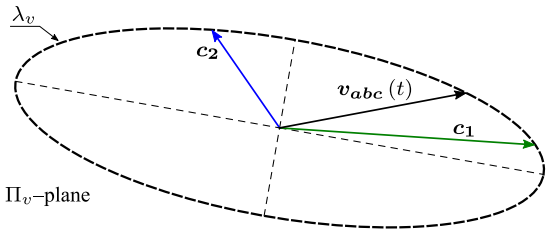

FIGURE 2. Voltage locus and Π_v–plane.

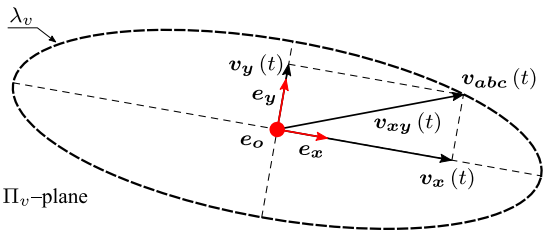

FIGURE 3. Voltage locus and *xyo* axes.

Note that V_{ph} and θ_{ph} can take any value. Thus, using the space vector representation proposed in [25] and [26], the three-dimensional vector $\boldsymbol{v_{abc}}(t)$ is defined as:

$$\boldsymbol{v_{abc}}(t) = [v_a(t), v_b(t), v_c(t)], \tag{2}$$

and this vector describes a three-dimensional trajectory over the time t.

This trajectory can be easily interpreted rewriting (2) as:

$$\boldsymbol{v_{abc}}(t) = \boldsymbol{c_1}\cos(\omega t) + \boldsymbol{c_2}\sin(\omega t), \tag{3}$$

since (2) is also the homogeneous solution of the harmonic oscillator extended to $\boldsymbol{v_{abc}}(t)$:

$$\frac{d^2\,\boldsymbol{v_{abc}}(t)}{d\,t^2} + \omega^2\,\boldsymbol{v_{abc}}(t) = 0. \tag{4}$$

where $\boldsymbol{c_1}$, $\boldsymbol{c_2}$ are constant vectors given by the initial conditions:

$$\boldsymbol{c_1} = \boldsymbol{v_{abc}}(t)\Big|_{t=0}, \tag{5}$$

$$\boldsymbol{c_2} = \frac{d}{dt}\left(\frac{\boldsymbol{v_{abc}}(t)}{\omega}\right)\Big|_{t=0}. \tag{6}$$

From (3) it is derived that the trajectory of $\boldsymbol{v_{abc}}(t)$ is in the plane defined by $\boldsymbol{c_1}$ and $\boldsymbol{c_2}$. Both, the orientation of that plane (hereinafter Π_v–plane) and the locus or the shape of the $\boldsymbol{v_{abc}}(t)$ trajectory (hereinafter λ_v–locus), depend on the degree of the voltage imbalance. Figure 2 shows a general case of voltage imbalance where the λ_v–locus described by $\boldsymbol{v_{abc}}(t)$ in the Π_v–plane and vectors $\boldsymbol{c_1}$ and $\boldsymbol{c_2}$ are illustrated. In [22], three classes associated with the locus shape were defined: circular (Class I), elliptical (Class II) and linear (Class III). Note that Class II (elliptical shape) is the most general case while the other two are degenerated versions of it.

The proposed RRF takes advantage of the locus-shape symmetry and geometrical properties. For this purpose, the RRF orientation is defined over the ellipse semi-major and semi-minor axes which are denominated in the transformation as x and y directions respectively. The orthonormal direction to the Π_v–plane is known as o direction defining the *xyo* axes of the RRF. As illustrated in Fig. 3, the RRF frame is defined by the set of orthonormal vectors $\{\boldsymbol{e_x}, \boldsymbol{e_y}, \boldsymbol{e_o}\}$. Note that $\boldsymbol{e_o}$ is pointing outward the Π_v–plane.

The components of $\boldsymbol{v_{abc}}(t)$ can be represented in the RRF as follows:

$$\boldsymbol{v_{xyo}}(t) = \left[v_x(t), v_y(t), v_o(t)\right] = T_{Rv}^{ext}\,\boldsymbol{v_{abc}}(t), \tag{7}$$

where T_{Rv}^{ext} is the unitary rotation matrix

$$T_{Rv}^{ext} = \begin{bmatrix} e_{xa} & e_{xb} & e_{xc} \\ e_{ya} & e_{yb} & e_{yc} \\ e_{oa} & e_{ob} & e_{oc} \end{bmatrix}, \tag{8}$$

and $\boldsymbol{e_x} = [e_{xa}, e_{xb}, e_{xc}]$, $\boldsymbol{e_y} = \left[e_{ya}, e_{yb}, e_{yc}\right]$ and $\boldsymbol{e_o} = [e_{oa}, e_{ob}, e_{oc}]$ are the coordinates of $\{\boldsymbol{e_x}, \boldsymbol{e_y}, \boldsymbol{e_o}\}$ expressed in the canonical base $\{[1,0,0], [0,1,0], [0,0,1]\}$ or the *abc* frame.

The resulting components $v_x(t)$, $v_y(t)$ and $v_o(t)$ are characterised by the following properties:

- Null value for the orthonormal component $v_o(t)$ since all the locus lies within the Π_v–plane. This property allows to use the reduced version of the transformation:

$$T_{Rv} = \begin{bmatrix} e_{xa} & e_{xb} & e_{xc} \\ e_{ya} & e_{yb} & e_{yc} \end{bmatrix}, \tag{9}$$

  where only xy are required to be computed:

$$\boldsymbol{v_{xy}}(t) = T_{Rv}\boldsymbol{v_{abc}}(t), \tag{10}$$

- The $v_x(t)$, $v_y(t)$ components are two sinusoidal functions $\pi/2$ radians out of phase (1/4 cycle), whose amplitudes are related with the eccentricity ε_v of the ellipse.

Since in a three-phase four-wire system there are at most three lineal independent line currents $i_a(t)$, $i_b(t)$, $i_c(t)$, a similar procedure can be applied to the currents to obtain the λ_i–locus, the Π_i–plane and the T_{Ri}^{ext} transform. Note that the subscript i is used to denote that the RRF transform is related to currents.

Once the voltages and currents have been defined in the same RRF, they can be used to formulate the active and reactive powers. In this work, the considered reference plane is Π_v, therefore the voltages and currents in the RRF are given respectively by (7) and

$$\boldsymbol{i_{xyo}}(t) = T_{Rv}^{ext}\,\boldsymbol{i_{abc}}(t). \tag{11}$$

The power definition is independent of the selected reference frame, thus, using the *abc* frame, the active power of the system, P, is defined as the sum of the active power of each phase, $P = P_a + P_b + P_c$

$$P = \Re\{\underline{V}_a\underline{I}_a^{\star}\} + \Re\{\underline{V}_b\underline{I}_b^{\star}\} + \Re\{\underline{V}_c\underline{I}_c^{\star}\}, \tag{12}$$

and the reactive power $Q = Q_a + Q_b + Q_c$

$$Q = \Im\{\underline{V}_a \underline{I}_a^\star\} + \Im\{\underline{V}_b \underline{I}_b^\star\} + \Im\{\underline{V}_c \underline{I}_c^\star\}, \tag{13}$$

where $\underline{V}_a$, $\underline{V}_b$, $\underline{V}_c$ are the phasors related to $v_a(t)$, $v_b(t)$, $v_c(t)$, and $\underline{I}_a^\star$, $\underline{I}_b^\star$, $\underline{I}_c^\star$ are the complex conjugate of the phasors related to $i_a(t)$, $i_b(t)$, $i_c(t)$.

Using the RRF transformation:

$$\begin{bmatrix} \underline{V}_x \\ \underline{V}_y \\ \underline{V}_o \end{bmatrix} = T_{Rv}^{ext} \cdot \begin{bmatrix} \underline{V}_a \\ \underline{V}_b \\ \underline{V}_c \end{bmatrix}, \tag{14}$$

$$\begin{bmatrix} \underline{I}_x \\ \underline{I}_y \\ \underline{I}_o \end{bmatrix} = T_{Rv}^{ext} \cdot \begin{bmatrix} \underline{I}_a \\ \underline{I}_b \\ \underline{I}_c \end{bmatrix}, \tag{15}$$

the powers are formulated as $P = P_x + P_y + P_o$,

$$P = \Re\{\underline{V}_x \underline{I}_x^\star\} + \Re\{\underline{V}_y \underline{I}_y^\star\} + \Re\{\underline{V}_o \underline{I}_o^\star\}, \tag{16}$$

and $Q = Q_x + Q_y + Q_o$,

$$Q = \Im\{\underline{V}_x \underline{I}_x^\star\} + \Im\{\underline{V}_y \underline{I}_y^\star\} + \Im\{\underline{V}_o \underline{I}_o^\star\}, \tag{17}$$

where $\underline{V}_x$, $\underline{V}_y$, $\underline{V}_o$ are the phasors related to $v_x(t)$, $v_y(t)$, $v_o(t)$ respectively and $\underline{I}_x^\star$, $\underline{I}_y^\star$, $\underline{I}_o^\star$ are the complex conjugate of the phasors related to $i_x(t)$, $i_y(t)$, $i_o(t)$ respectively.

The instantaneous active and reactive power can be expressed according to [27] in *abc* and RRF axes as follows:

$$p(t) = \boldsymbol{v_{abc}}(t) \cdot \boldsymbol{i_{abc}}(t) = \boldsymbol{v_{xy}}(t) \cdot \boldsymbol{i_{xyo}}(t), \tag{18}$$

$$q(t) = \|\boldsymbol{q_{abc}}(t)\| = \|\boldsymbol{q_{xyo}}\| = \|\boldsymbol{v_{xy}}(t) \times \boldsymbol{i_{xyo}}(t)\| \tag{19}$$

The power computation using the RRF presents a key advantage with respect to the *abc* frame, as the component v_o is always null. This allows to obtain a reduced expression for the active power P, reactive power Q and instantaneous active power,

$$P = P_x + P_y = \Re\{\underline{V}_x \underline{I}_x^\star\} + \Re\{\underline{V}_y \underline{I}_y^\star\}, \tag{20}$$

$$Q = Q_x + Q_y = \Im\{\underline{V}_x \underline{I}_x^\star\} + \Im\{\underline{V}_y \underline{I}_y^\star\}, \tag{21}$$

$$p(t) = v_x i_x + v_y i_y. \tag{22}$$

However, this reduction is not achieved for the instantaneous reactive power since i_o affects the voltages in xy axes:

$$\boldsymbol{q_{xyo}}(t) = \begin{bmatrix} v_y i_o \\ -v_x i_o \\ v_x i_y - v_y i_x \end{bmatrix}, \tag{23}$$

$$q(t) = \sqrt{i_o^2 \left(v_x^2 + v_y^2\right) + \left(v_x i_y - v_y i_x\right)^2}. \tag{24}$$

Despite a reduction in the reactive power terms is not achieved, its computation is simpler than in the *abc* frame since the v_o component is always null.

In the case of Π_v and Π_i are coincident, the component i_o would be null. As a consequence, the instantaneous reactive power is reformulated as $q(t) = \|q_o(t)\|$:

$$q_o(t) = v_x i_y - v_y i_x. \tag{25}$$

This allows to represent the instantaneous active and reactive power in a compact form as follows:

$$\begin{bmatrix} p(t) \\ q_o(t) \end{bmatrix} = \begin{bmatrix} v_x & v_y \\ -v_y & v_x \end{bmatrix} \begin{bmatrix} i_x \\ i_y \end{bmatrix}. \tag{26}$$

Equation (26) allows to adopt a complex formulation similar to the one presented in [8], but extending its application to voltages and currents including zero–sequence components:

$$p(t) + j\, q_o(t) = \underline{v}_{xy}^\star(t)\ \underline{i}_{xy}(t), \tag{27}$$

where

$$\underline{v}_{xy}^\star(t) = v_x(t) - j v_y(t),$$
$$\underline{i}_{xy}(t) = i_x(t) + j i_y(t).$$

III. CASE STUDIES

This section presents two case studies for evaluating the performance of the RRF transform in comparison with the classical $\alpha\beta\gamma$ frame and the recent *mno* coordinates proposed by Montanari and Gole [17]. For this, the 3-phase 4-wire circuit depicted in Fig. 1 is analyzed with voltage and load imbalance conditions as reported in the following subsections.

A. VOLTAGE IMBALANCE

This case study considers a balanced load fed from an unbalanced voltage source. In this case, the line currents circulating through the load can be computed as follows:

$$\begin{bmatrix} \underline{I}_a \\ \underline{I}_b \\ \underline{I}_c \end{bmatrix} = \frac{1}{(R + jX)} \begin{bmatrix} 1 & 0 & 0 \\ 0 & 1 & 0 \\ 0 & 0 & 1 \end{bmatrix} \begin{bmatrix} \underline{V}_a \\ \underline{V}_b \\ \underline{V}_c \end{bmatrix}, \tag{28}$$

with

$$R + jX = \underline{Z} = Z e^{j\varphi_Z} = \sqrt{R^2 + X^2}\, e^{j\left(\arctan \frac{X}{R}\right)}. \tag{29}$$

where it is observed that each current phasor is proportionally scaled and delayed in an identical manner with respect to its voltage phasor. Applying the RRF transformation, defined in (7) and (8), to the voltage and current phasors in (28), leads to:

$$\begin{bmatrix} \underline{V}_x \\ \underline{V}_y \\ \underline{V}_o \end{bmatrix} = \left[T_{Rv}^{ext}\right] \begin{bmatrix} \underline{V}_a \\ \underline{V}_b \\ \underline{V}_c \end{bmatrix} = \begin{bmatrix} V_x e^{j\varphi_{V_x}} \\ V_y e^{j(\varphi_{V_x} - \pi/2)} \\ 0 \end{bmatrix}, \tag{30}$$

$$\begin{bmatrix} \underline{I}_x \\ \underline{I}_y \\ \underline{I}_o \end{bmatrix} = \left[T_{Rv}^{ext}\right] \begin{bmatrix} \underline{I}_a \\ \underline{I}_b \\ \underline{I}_c \end{bmatrix} = \frac{1}{Z} \begin{bmatrix} V_x e^{j(\varphi_{V_x} - \varphi_Z)} \\ V_y e^{j(\varphi_{V_x} - \pi/2 - \varphi_Z)} \\ 0 \end{bmatrix}. \tag{31}$$

The instantaneous voltage $v_{xyo}(t)$ and current $i_{xyo}(t)$ are computed as:

$$\begin{bmatrix} v_x(t) \\ v_y(t) \\ v_o(t) \end{bmatrix} = \begin{bmatrix} \sqrt{2} V_x \cos\left(\omega t + \varphi_{V_x}\right) \\ \sqrt{2} V_y \sin\left(\omega t + \varphi_{V_x}\right) \\ 0 \end{bmatrix}, \tag{32}$$

$$\begin{bmatrix} i_x(t) \\ i_y(t) \\ i_o(t) \end{bmatrix} = \begin{bmatrix} \sqrt{2}\left(V_x/Z\right) \cos\left(\omega t + \varphi_{V_x} - \varphi_z\right) \\ \sqrt{2}\left(V_y/Z\right) \sin\left(\omega t + \varphi_{V_x} - \varphi_z\right) \\ 0 \end{bmatrix}. \tag{33}$$

Note that the values of $v_o(t)$ and $i_o(t)$ are null, therefore, the voltage and current loci of the vectors $\boldsymbol{v}(t)$, $\boldsymbol{i}(t)$ are in the same plane. As a result, it can be stated that irrespective of the voltage imbalance, the Π_v and Π_i planes are coincident when the load is balanced. In addition, $\underline{V}_y$ and $\underline{I}_y$ lag $\pi/2$ with respect to $\underline{V}_x$ and $\underline{I}_x$, respectively. This means that λ_v and λ_i are two ellipses with aligned semi-major and semi-minor axes. The eccentricity ε_v of λ_v is given by the amplitude of $v_x(t)$ and $v_y(t)$:

$$\varepsilon_v = \sqrt{1 - \left(\frac{V_y}{V_x}\right)^2}. \tag{34}$$

Note that, considering (33), $\varepsilon_v = \varepsilon_i$. As a consequence, λ_v and λ_i are concentric since both loci have the same semi-major and semi-minor axes. This feature holds for balanced loads irrespective of whether the voltage is balanced or not.

The formulation of the different power definitions provided by (20), (21) and (26) can be particularized as a function of the voltage, load impedance and eccentricity as follows:

$$P = \left(2 - \varepsilon^2\right)\left(V_x^2/Z\right)\cos\varphi_Z, \tag{35}$$

$$Q = \left(2 - \varepsilon^2\right)\left(V_x^2/Z\right)\sin\varphi_Z, \tag{36}$$

$$\begin{bmatrix} p(t) \\ q(t) \end{bmatrix} = \begin{bmatrix} P + \varepsilon^2\left(V_x^2/Z\right)\cos\left(2\omega t + 2\varphi_{V_x} - \varphi_Z\right) \\ \|2\sqrt{1-\varepsilon^2}\left(V_x^2/Z\right)\sin\varphi_Z\| \end{bmatrix} \tag{37}$$

Note that $q(t)$ has a constant value only affected by V_x, φ_Z and ε. Whereas, $p(t)$ is composed by a constant value P and cosine function $\tilde{p}\,(t)$ with twice the angular frequency.

These theoretical analysis can be complemented in a numerical way considering two test cases with different voltage imbalances: (i) voltage with positive and negative sequences (PNV case) and (ii) voltage with positive, negative and zero sequences (PNVZ case). The symmetrical components of the voltages for these two case studies are set as follows:

$$\underline{\boldsymbol{V}}_{\mathbf{012}}^{\boldsymbol{PNV}} = \underline{V}\begin{bmatrix} 0 \\ 1 \\ k\,\underline{k}_2 \end{bmatrix}, \tag{38}$$

$$\underline{\boldsymbol{V}}_{\mathbf{012}}^{\boldsymbol{PNZV}} = \underline{V}\begin{bmatrix} k\,\underline{k}_0 \\ 1 \\ \frac{\underline{k}_2}{2} \end{bmatrix}, \tag{39}$$

where $\{\underline{V}, \underline{k}_0, \underline{k}_2\} \in \mathbb{C}$ are constant values, and $k \in [0, 1)$ is a sweep variable. Note that in this way, it is possible to analyze how the variation of the voltage imbalance affects the transformation results. The numerical analysis considers $\{\underline{V}, \underline{k}_0, \underline{k}_2\} = \{\frac{224.4}{\sqrt{2}}\angle 0\ \text{V}, 1\angle -\frac{\pi}{2}, 1\angle -\frac{\pi}{2}\}$. Figure 4 depicts in the phasor domain the voltages $\underline{\boldsymbol{V}}_{\mathbf{012}}^{\boldsymbol{PNV}}$ and $\underline{\boldsymbol{V}}_{\mathbf{012}}^{\boldsymbol{PNZV}}$ for $k = \{0, 0.25, 0.5, 0.75, 1\}$. These voltages are easily transformed to the *abc* frame through the Fortescue Transform [28], [29]:

$$\underline{\boldsymbol{V}}_{\boldsymbol{abc}} = [T_F]^{-1}\,\underline{\boldsymbol{V}}_{\mathbf{012}} = \begin{bmatrix} 1 & 1 & 1 \\ 1 & \underline{\alpha}^2 & \underline{\alpha} \\ 1 & \underline{\alpha} & \underline{\alpha}^2 \end{bmatrix}\underline{\boldsymbol{V}}_{\mathbf{012}}, \tag{40}$$

where $\underline{\alpha} = e^{j\frac{2\pi}{3}}$.

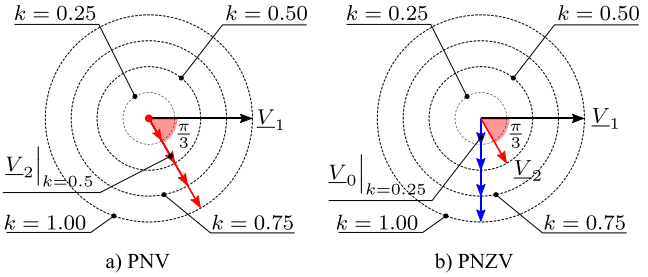

FIGURE 4. Symmetrical components of PNV and PNZV source imbalance.

The numerical analysis presented in the next subsections assume a balanced load for the PNV and PNVZ cases: $R_a = R_b = R_c = R = 120\ \Omega$, $X_a = X_b = X_c = X = 2\pi fL$, with $f = 50$ Hz and $L = 1.2$ H.

1) PNV VOLTAGE IMBALANCE

The PNV case aims to study how the negative sequence affects the voltage and current loci within the $\alpha\beta\gamma$, *mno* and *xyo* reference frames. In this case, k is the ratio between the positive and negative sequence components. The locus variation and voltages over time in the $\alpha\beta\gamma$, *mno* and *xyo* reference frames for $k = \{0, 0.5, 1.0\}$ in the PNV case are shown in Fig. 5. The first row within Fig. 5 presents the results in the $\alpha\beta\gamma$ and *mno* reference frames while the second row shows the voltage in the *xyo* reference frame. In this figure, the first column shows the voltage loci in each reference frame and the rest of the columns present the voltage components for the different unbalance parameter k.

Note that for $k = 0$, the voltage locus is circular in all the reference frames, being the Π-plane, the $\alpha\beta$-plane and *mno*-plane coincident. Moreover, the *mno* axes have the same orientation than the $\alpha\beta\gamma$ axes. This is because the objective of the *mno* transform is to contain the transformed-magnitude locus within the $\alpha\beta$-plane. It is interesting to note that, due to the circular voltage locus, it is possible to select the *xyo* to be coincident with the $\alpha\beta\gamma$ and *xyo* reference frames, since the semi-major and semi-minor axes have the same length. As a result, the time evolution of the voltage components is identical for all the reference frames, as shown in the second column of the Fig. 5.

For $k > 0$, the locus eccentricity increases approaching gradually to the linear locus. In these cases, a remarkable difference between the transformations appears since the $\alpha\beta\gamma$ and *mno* axis remains in the same position independently of the imbalance type. On the contrary, the *xyo* axis are oriented with the ellipse semi-major and semi-minor axes adapting to the specific unbalance voltage. As a result, the voltage components in the *xyo* axes remain with a phase difference of $\pi/2$ radians while those of $\alpha\beta\gamma$ and *mno* depend on the imbalance. Moreover, it is important to point out that the *mno* transform is not defined for the linear locus, i.e. $k = 1$, as shown in the fourth column of Fig. 5.

Finally, it is worth noting that, due to the absence of zero-sequence components, the voltages related to γ and o

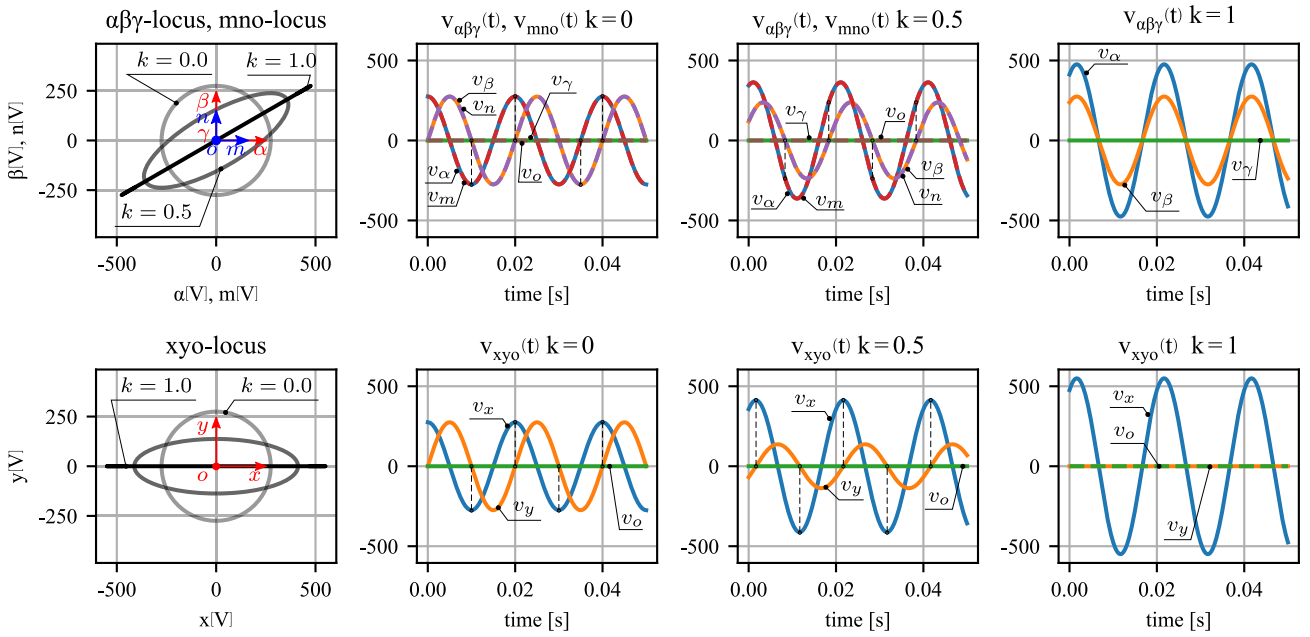

FIGURE 5. PNV voltage source imbalance. Voltage loci in $\alpha\beta\gamma$, *mno* and *xyo* reference frames.

components are zero regardless of the negative sequence imbalanced defined by k.

The current loci follows a similar trend than the voltage one since, according to (33), the current components are just scaled and delayed with respect to the voltages. Considering voltage and current loci in each of the transformation axes, the instantaneous values of $p\,(t)$ and $q\,(t)$, defined according to (37), are presented in Fig. 6 for $k = \{0, 0.5, 1\}$. As expected, constant values of $p\,(t)$ and $q\,(t)$ are obtained for $k = 0$ due to the balanced conditions of voltage and load. On the contrary, $p\,(t)$ is no longer constant for $k > 0$, which oscillates at 100 Hz. However, it is interesting to note that $q\,(t)$ is constant irrespective of the negative sequence content. Moreover, $q\,(t)$ is null for $k = 1$ since $\boldsymbol{v_{xy}}\,(t)$ and $\boldsymbol{i_{xyo}}\,(t)$ are parallel each other (linear locus), being the cross product in eq. (19) equal to zero.

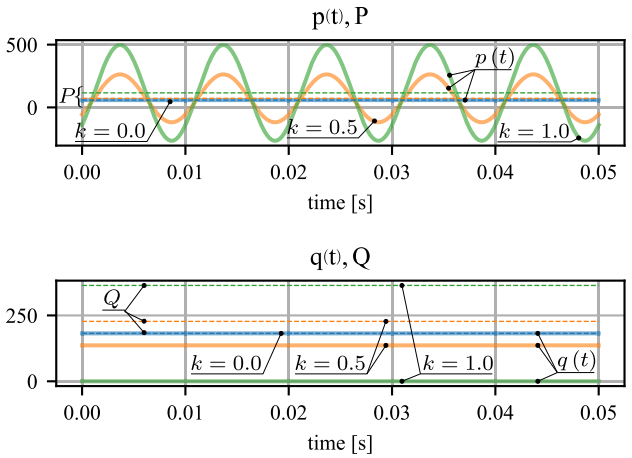

FIGURE 6. PNV voltage source imbalance. Instantaneous power $\boldsymbol{p(t)}$, $\boldsymbol{q(t)}$ (solid lines). Active and reactive powers $\boldsymbol{P}$, $\boldsymbol{Q}$ (dashed lines). $\boldsymbol{k = 0.0}$ (blue color), $\boldsymbol{k = 0.5}$ (orange color) and $\boldsymbol{k = 1.0}$ (green color).

2) PNZV VOLTAGE IMBALANCE

The PNZV case aims to study the influence of the zero sequence component in $\alpha\beta\gamma$, *mno* and *xyo* reference frames considering constant positive and negative sequence components. In this case, k is the ratio between the positive and zero sequence components.

Fig. 7 illustrates the voltages in each of the analyzed reference frames. Note that the figure contains three rows since the voltage loci within the *mno* reference frame is no longer equal to the corresponding loci on in $\alpha\beta\gamma$ axes. The results for $k = 0$ leads to the conclusions pointed out in the previous subsection due to the absence of zero-sequence component. The zero-sequence component is responsible of a non-null γ component in the conventional $\alpha\beta\gamma$ reference frame as shown in Fig. 7 for $k > 0$. On the contrary, the *mno* and *xyo* transformations are able to describe the imbalance voltage just with two components due to their capability of adapting to the voltage imbalance. With this regard, it can be stated the superior performance of the *xyo* reference frame with respect to the *mno* axes since the voltage components remain always orthogonal irrespective of the zero-sequence voltage content.

The active and reactive instantaneous power for this PNVZ case are shown in Fig. 8. Evidently, the instantaneous active power maintains the oscillatory component at 100 Hz while the instantaneous reactive power remains constant. This is because, as shown in (33), voltage and current loci have the same eccentricity.

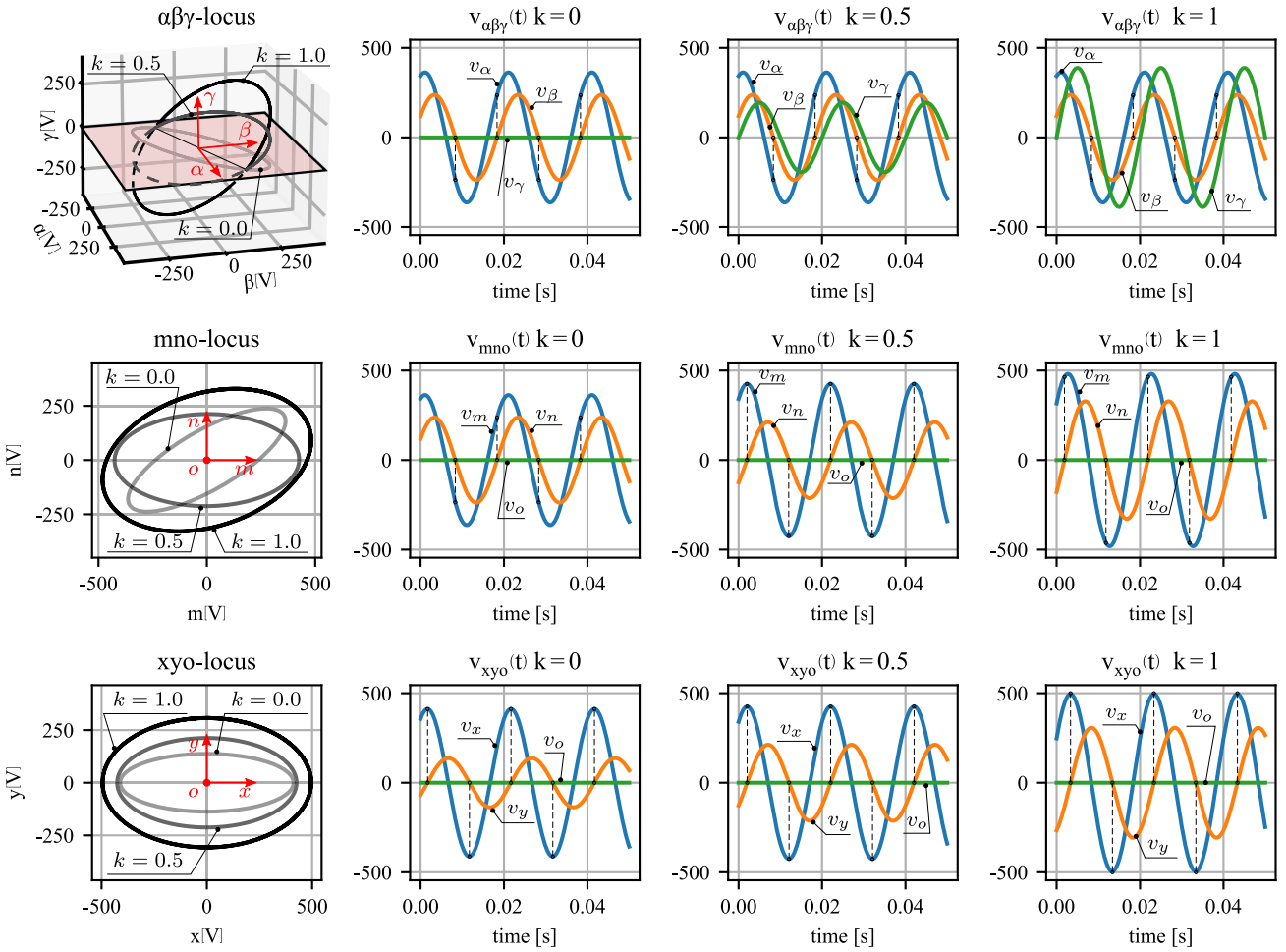

FIGURE 7. PNZV source imbalance. Voltages in $\alpha\beta\gamma$, *mno* and *xyo* reference frames.

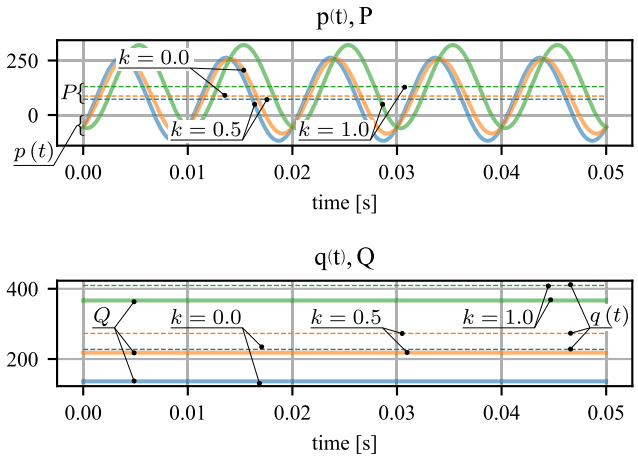

FIGURE 8. PNZV source imbalance. Instantaneous power $p(t)$, $q(t)$ (solid lines). Active and reactive powers P, Q (dashed lines). $k = 0.0$ (blue color), $k = 0.5$ (orange color) and $k = 1.0$ (green color).

B. LOAD IMBALANCE

This case considers balanced voltages and unbalanced loads in the system depicted in Fig. 1. The load current can be formulated in a matrix form as:

$$\underline{\boldsymbol{I}}_{\boldsymbol{abc}} = \underline{Y}_{abc}\,\underline{\boldsymbol{V}}_{\boldsymbol{abc}}, \tag{41}$$

where Y_{abc} is the admittance matrix. These currents can be represented in the RRF applying the voltage-based transformation matrix T_{Rv}^{ext} as:

$$\underline{\boldsymbol{I}}_{\boldsymbol{xyo}} = T_{Rv}^{ext}\,\underline{Y}_{abc}\left[T_{Rv}^{ext}\right]^{T}\underline{\boldsymbol{V}}_{\boldsymbol{xyo}} = \underline{Y}_{xyo}\,\underline{\boldsymbol{V}}_{\boldsymbol{xyo}}. \tag{42}$$

The relationship between the admittance matrices, $\underline{Y}$, formulated in the *abc* frame, symmetrical components and *xyo* coordinates are illustrated in Fig. 9.

In case of a balanced voltage, the corresponding loci in the RRF is circular and $\underline{V}_x$ and $\underline{V}_y$ are signals delayed $\pi/2$ radians with equal amplitude:

$$\begin{bmatrix} v_x(t) \\ v_y(t) \end{bmatrix} = \begin{bmatrix} \sqrt{2}V_x \cos\left(\omega t + \varphi_{V_x}\right) \\ \sqrt{2}V_x \cos\left(\omega t + \varphi_{V_x} - \pi/2\right) \end{bmatrix}. \tag{43}$$

Moreover, it is worth noting to note that the x and y axes can be located in multiple positions due to the circular loci as shown Fig. 10. This figure also depicts a general case where the current plane Π_i is not oriented with the voltage

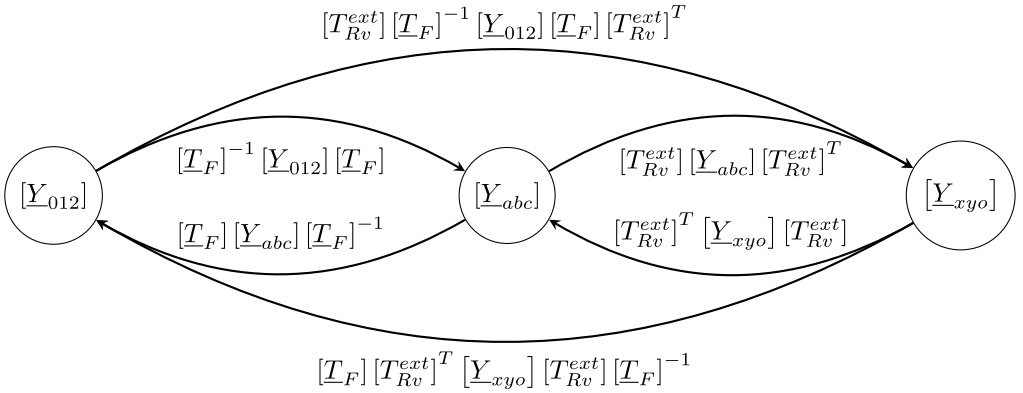

FIGURE 9. $\underline{Y}$ **matrix transformations.**

plane Π_v. With the aim of simplifying as much as possible the mathematical formulation, the x and y axes are aligned with the semi-major and semi-minor axis of the projected current loci, projλ_i, in the voltage plane Π_v, as shown in Fig. 10. Note that, in this way, the x and y current components are related by the loci eccentricity in a similar manner than (34):

$$I_y = I_x\sqrt{1-\epsilon_i^2}. \tag{44}$$

Therefore, the current formulated in the xyo coordinates can be expressed as

$$\begin{bmatrix}\underline{I}_x\\ \underline{I}_y\\ \underline{I}_o\end{bmatrix} = \underline{V}_x\begin{bmatrix}\underline{y}_{xx}-j\underline{y}_{yx}\\ \underline{y}_{xy}-j\underline{y}_{yy}\\ \underline{y}_{xo}-j\underline{y}_{yo}\end{bmatrix}, \tag{45}$$

and

$$\begin{bmatrix}i_x(t)\\ i_y(t)\\ i_o(t)\end{bmatrix} = \begin{bmatrix}\sqrt{2}I_x\cos\left(\omega t+\varphi_{I_x}\right)\\ \sqrt{2}I_y\cos\left(\omega t+\varphi_{I_x}-\pi/2\right)\\ \sqrt{2}I_o\cos\left(\omega t+\varphi_{I_o}\right)\end{bmatrix}, \tag{46}$$

where $\underline{y}_{jk}$ with $j,k \in \{x,y,o\}$ corresponds to the different terms of the admittance matrix $\underline{Y}_{xyo}$. Note that the currents $i_x(t)$ and $i_y(t)$ are in quadrature, and in addition, the current $\underline{I}_o$ is not null in a general case meaning that the current and voltage loci are in different planes.

According (20), (21), (22) the power terms $P, Q, p\,(t)$ only depends on x and y components since the voltage v_o is always null. Therefore these power terms can be computed in this particular case as follows:

$$P = V_xI_x\left(1+\sqrt{1-\epsilon_i^2}\right)\cos\varphi, \tag{47}$$

$$Q = V_xI_x\left(1+\sqrt{1-\epsilon_i^2}\right)\sin\varphi, \tag{48}$$

$$p(t) = P+\tilde{p}(t), \tag{49}$$

$$\tilde{p}(t) = V_xI_x\left(1-\sqrt{1-\epsilon_i^2}\right)\cos\left(2\omega t+2\varphi_{V_x}-\varphi\right), \tag{50}$$

where

$$\varphi = \varphi_{V_x}-\varphi_{I_x}. \tag{51}$$

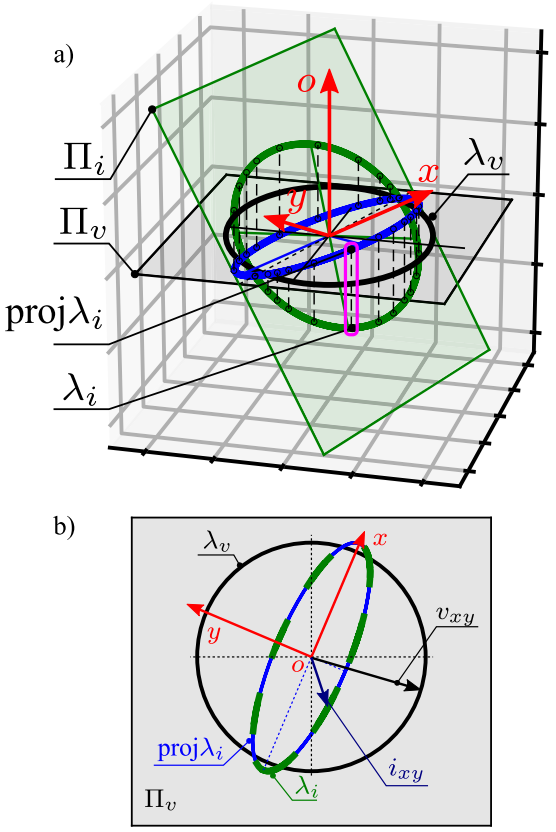

FIGURE 10. **Locus of current and its projection into the plane of voltages for unbalanced load and balanced voltages.**

On the other hand, $q\,(t)$ is a function of $i_o\,(t)$, as stated in (24). For this particular case with balanced voltages, the instantaneous reactive power can be formulated as:

$$q\,(t) = V_x\sqrt{f_1(t)+f_2(t)+f_3(t)+C_1+C_2+C_3}, \tag{52}$$

where $f_1(t), f_2(t), f_3(t)$ are oscillatory terms and C_1, C_2, C_3 are constant terms:

$$f_1(t) = 4\,I_o^2\cos\left(2\omega t+2\varphi_{I_o}\right),$$
$$f_2(t) = 2\,(\sin\varphi)\,(I_x\epsilon_i)^2\sin\left(2\omega t+2\varphi_{V_x}-\varphi\right),$$

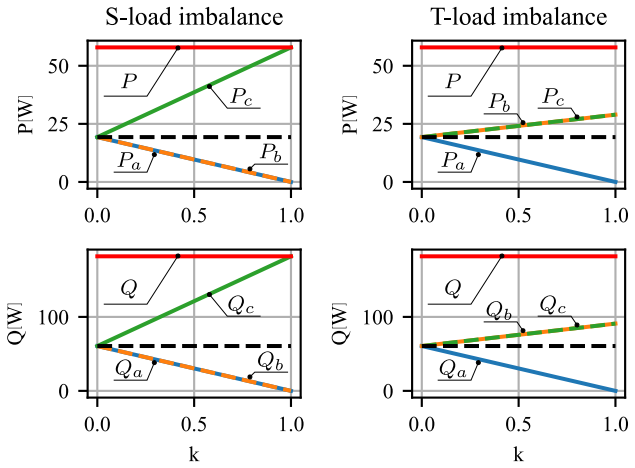

FIGURE 11. Active and reactive power for the S-type and T-type loads versus the imbalance factor *k*.

$$f_3(t) = \frac{-I_x^2}{2}\left(1-\sqrt{1-\epsilon_i^2}\right)^2 \cos\left(4\omega t + 4\varphi_{V_x} - 2\varphi\right),$$
$$C_1 = 2\,I_o^2,$$
$$C_2 = (2\,I_x \sin\varphi)^2\sqrt{1-\epsilon_i^2},$$
$$C_3 = \left(I_x\left(1-\sqrt{1-\epsilon_i^2}\right)\right)^2\left(\frac{1}{2}+\sin^2(\varphi)\right).$$

Note that $q\,(t)$ is periodic and non-negative.

In order to evaluate numerically the previous theoretical formulation, two types of load imbalance, one that tends to a single-phase load and other that tends to a two-phase load, namely type S and type T respectively, are considered with the following admittance matrices:

$$\underline{Y}^S_{abc} = \frac{1}{(R+jX)}\begin{bmatrix} 1-k & 0 & 0 \\ 0 & 1-k & 0 \\ 0 & 0 & 1+2k \end{bmatrix}, \quad (53)$$

and

$$\underline{Y}^T_{abc} = \frac{1}{(R+jX)}\begin{bmatrix} 1-k & 0 & 0 \\ 0 & 1+k/2 & 0 \\ 0 & 0 & 1+k/2 \end{bmatrix}, \quad (54)$$

where $k \in [0, 1)$ is a sweep variable which control the imbalance degree. Note that for $k = 0$, type S and type T loads perform like a perfectly balance load, while for $k = 1$ are a single-phase and two-phase loads respectively as shown in Fig. 11. This numerical analysis has been done assuming a perfectly 50 Hz balanced three-phase voltage source with amplitude 224.4 V, $R = 120\ \Omega$ and $L = 1.2$ mH. Note that in both cases the total active and reactive power load remain constant but, depending on the imbalance degree, this load is shared unevenly between the phases.

The next subsections are devoted to evaluate these two types of load imbalance in the different reference frames.

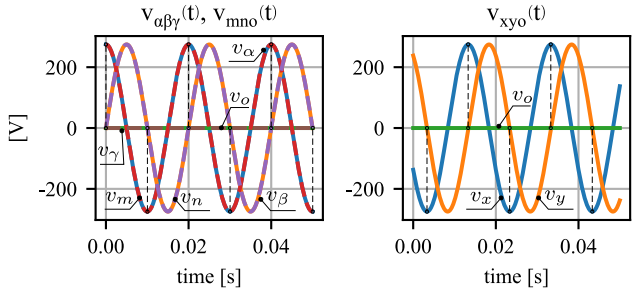

FIGURE 12. Voltages in $\alpha\beta\gamma$ and in *xyo* for any k value for load imbalance type S.

1) S-TYPE LOAD IMBALANCE

This subsection analyzes the current loci in the $\alpha\beta\gamma$, *mno* and *xyo* reference frames for the S type load with $k = \{0, 0.5, 1.0\}$. This analysis just refers to currents since the voltage is assumed balanced and constant in all the analyzed cases. In fact, the voltage locus and the voltage components in each reference frame are exactly the same that the ones shown in Fig. 12.

Given this voltage, the *mno* axes are the same than the conventional $\alpha\beta\gamma$ ones. For this reason, the current loci and the corresponding current components in these axes for any unbalance factor k are exactly the same, as shown in Fig. 13. Regarding the *xyo* transformation, the reference frame axes are aligned with the semi-major and semi-minor axes of the projection of the current loci on the voltage plane, as previously stated, to take advantage of the straightforward computation of the power terms using (47)-(51). For this reason, the current components in the x and y axes are delayed with respect to their counterparts in the *mno* and $\alpha\beta\gamma$ axes.

If the load imbalance increases, $k = 0.5$, the current loci is out of the voltage plane and, consequently the third current, i.e. i_γ and i_o, orthogonal to the voltage plane appears in all the transformations. Moreover, the imbalance increases the eccentricity of the current locus, which modifies the phase difference between the current components in the *mno* and $\alpha\beta\gamma$ reference frame. On the contrary, the current components in the *xyo* frame remain with a phase difference of $\pi/2$ radians due to a suitable axes alignment. Finally, in the case of a single-phase load, i.e. $k = 1$, it is interesting to note that $i_y = 0$ in the *xyo* transformation being the current locus described just with i_x and i_o which are in phase denoting a linear locus.

The power terms related to these current components for the different unbalance degrees of the S-type load are shown in Fig. 14. As expected, the instantaneous active power remains constant for the balance case, $k = 0$, but starts oscillating with the load imbalance, i.e. $\epsilon_i > 0$, according to (50). It is interesting to note that the total active power is constant for all the cases, which is consistent with the results shown in Fig. 11. Therefore, considering (44) and (47), the term $I_x\left(1+\sqrt{1-\epsilon_i^2}\right)$ which is equal to $I_x + I_y$ is constant irrespective of the imbalance factor, as shown in

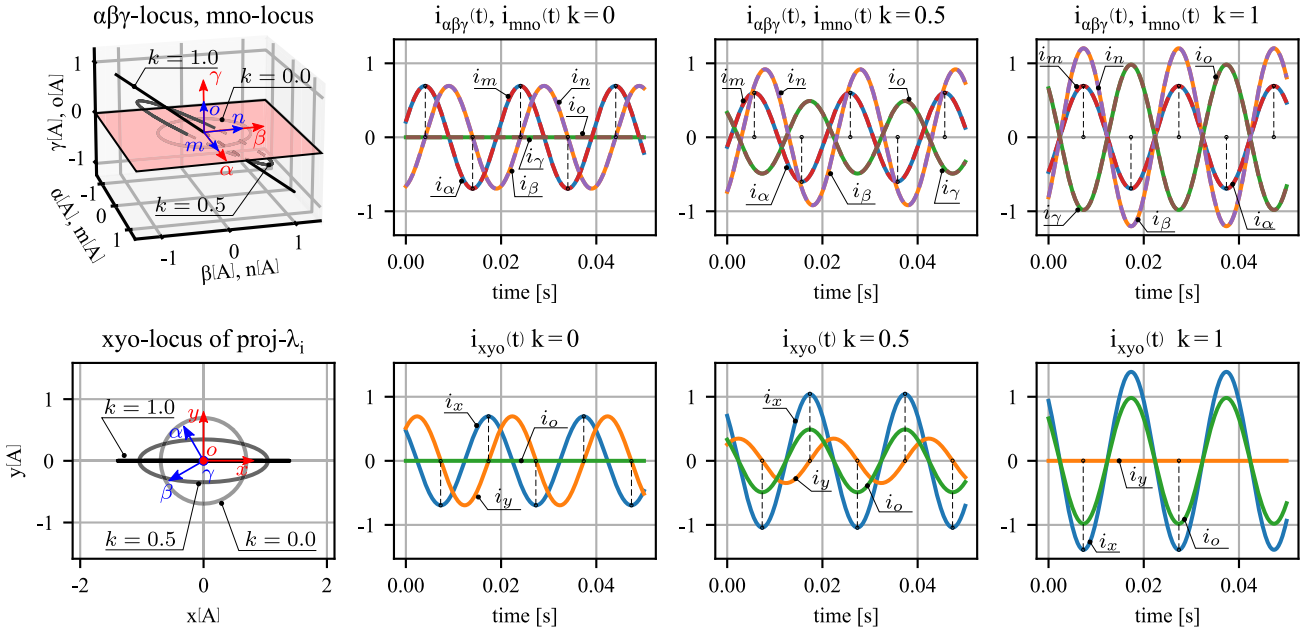

FIGURE 13. Currents in $\alpha\beta\gamma$, *mno* and *xyo* for the S-type load imbalance.

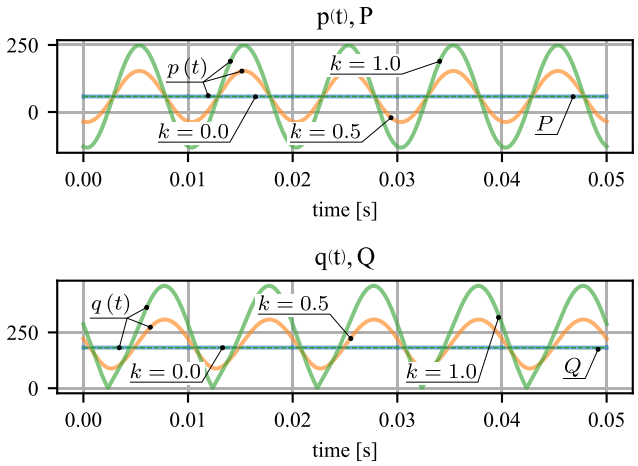

FIGURE 14. S-type load imbalance. Instantaneous power $p(t)$, $q(t)$ (solid lines). Active and reactive powers P, Q (dashed lines). $k = 0.0$ (blue color), $k = 0.5$ (orange color) and $k = 1.0$ (green color).

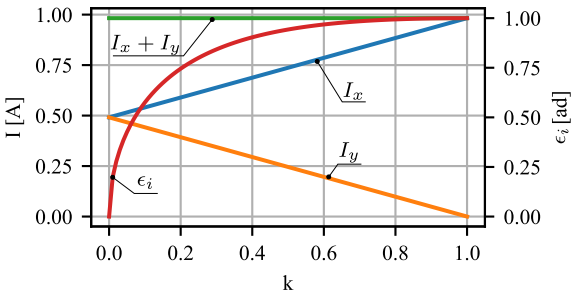

FIGURE 15. S-type load imbalance. Evolution of I_x, I_y and ϵ_i versus the imbalance factor k.

Fig. 15. The eccentricity of the current locus increases with the unbalance factor k which modifies the amplitudes of I_x and I_y but their sum remains constant. Note that for $k = 1$ $I_y = 0$ as shown in the fourth column of Fig. 13. Finally, the analysis of the reactive power deserve special attention. On the one hand, the total reactive power remains constant which can be justified in a similar manner than the previous analysis for the total active power but considering (48). On the other hand, the instantaneous reactive power is not constant like in the previously analyzed case of unbalanced voltages and balanced loads. Particularly, it is a periodic but non-linear function which is consistent with (52). Moreover, it is worth noting that the total reactive power Q is not the average value of $q(t)$ for $k > 0$.

2) T-TYPE LOAD IMBALANCE

This section analyzes the current loci in the different reference frames for the T-Type load imbalance with the results shown in Fig. 16. Again, the $\alpha\beta\gamma$ and *xyo* axes are coincident while the *xyo* ones adapt to the current imbalance. As a result, x and y components are always orthogonal irrespective of the current imbalance. However, it is worth noting that the eccentricity of the projected current locus in the *xyo* reference frame is lower than the one of the S-type load. Note that for the S-type load and $k = 1$ the current locus is a line, as shown in Fig. 13, while for the T-type load and $k = 1$ the current loci is an ellipse, as depicted in the first column of Fig. 16.

The different power components follow a similar trend than the ones previously presented as shown in Fig. 17 and, therefore, similar conclusions can be drawn. However, the main difference is related with the lower eccentricity of the projected current loci. As a matter of fact, $\epsilon < 1$ for the T-type load and maximum imbalance degree $k = 1$ as shown in Fig. 18. Therefore, considering a given unbalance factor k,

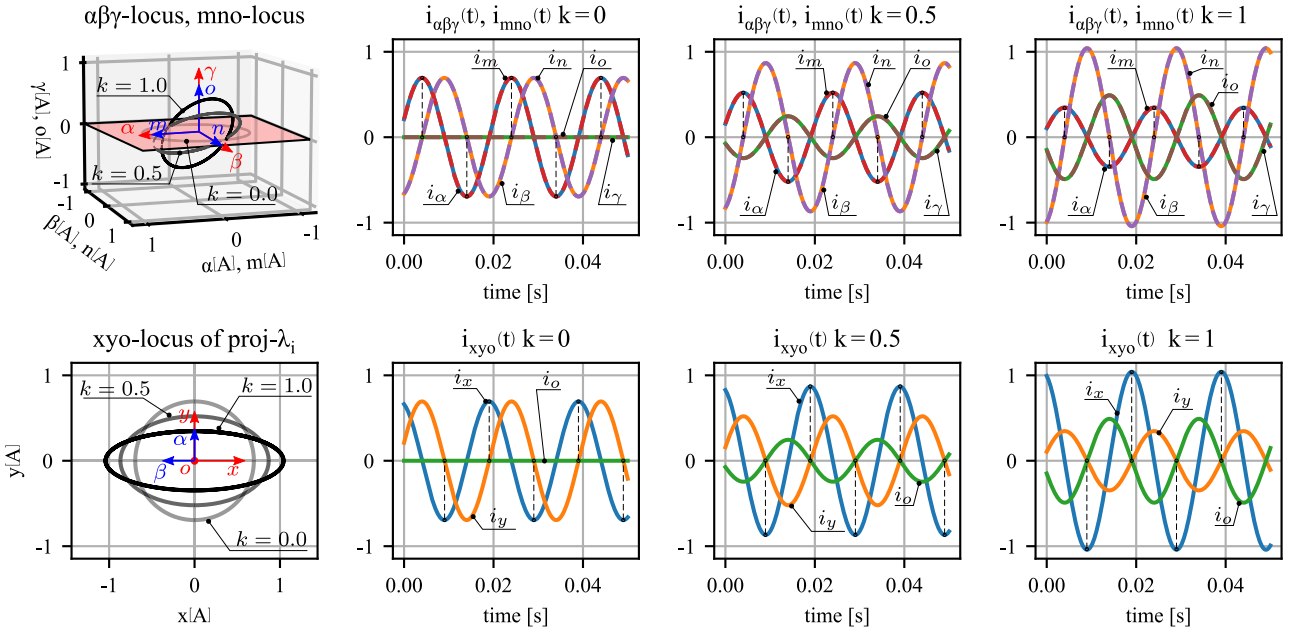

FIGURE 16. Currents in $\alpha\beta\gamma$, *mno* and in *xyo* load imbalance type T.

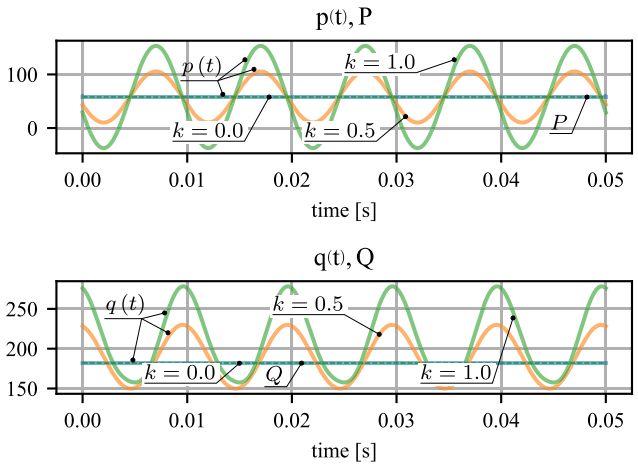

FIGURE 17. T-type load imbalance. Instantaneous power $p(t)$, $q(t)$ (solid lines). Active and reactive powers P, Q (dashed lines). $k = 0.0$ (blue color), $k = 0.5$ (orange color) and $k = 1.0$ (green color).

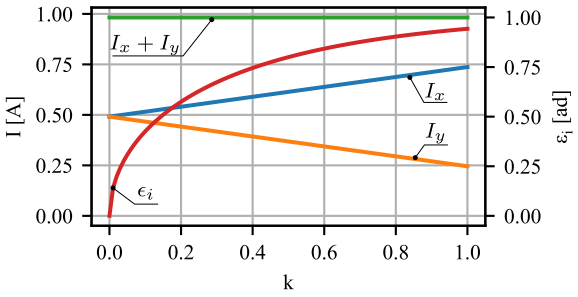

FIGURE 18. S-type load imbalance. Evolution of I_x, I_y and ϵ_i versus the imbalance factor k.

the power oscillating term of the instantaneous power is lower than the corresponding one of the S-tpye load, which is consistent with (46). Moreover, Fig. 18 also reveals the lower difference between the values of I_x and I_y shown in Fig. 16.

IV. CONCLUSION

This paper has analyzed the performance of the RRF transformation in different unbalance conditions of 3-phase and 4-wires systems. Particularly, this transform has been compared to the classical $\alpha\beta\gamma$ and the recent *mno* transformations to highlight its benefits in terms of imbalance classification and computation of the different power terms. For this purpose, two case studies with different imbalance conditions are studied: (i) unbalance voltage with balanced load and (ii) balanced voltage with unbalance load.

In the first case, the influence of the negative- and zero-sequence voltage components have been studied separately. Regardless of the voltage imbalance, it has been demonstrated that the voltage and the current planes are coincident, and in addition, their loci are concentric due to the balance characteristic of the load. Therefore, only two coordinates are needed to work with voltages and currents. Note that this is not the case for the $\alpha\beta\gamma$, where a third voltage component appears in case of zero-sequence voltage. In spite of the *mno* component is able to transform the voltage within a plane, even in case of zero-sequence voltages, it is worth noting that voltage components do not maintain a constant phase delay. In addition, this reference frame is not able to represent some imbalance scenarios such as those leading to a linear locus. On the contrary, the RRF transformation adapts properly the reference axes to achieve a constant phase $\pi/2$ delay between the voltage components irrespective of the imbalance content. Regarding the power components, all the power terms have been formulated as a function of some

properties of the voltage locus (V_x and ε) and the load (Z and φ_Z). The major finding is that, in case of a balanced load, the instantaneous reactive is constant irrespective of the voltage imbalance. Moreover, the computation of all the power terms is quite simple because just the x and y voltage and current components have to be considered.

The second case has studied a system composed of a balanced voltage source with two types of unbalanced loads, i.e. S-type and T-type load reproducing the performance of single- and two-phase load imbalance respectively. In this case, the voltage and current planes are no longer the same and, therefore, the third current component in the o axis appears in a similar manner than in the $\alpha\beta\gamma$ and mno reference frame. However, the RRF still maintains the constant $\pi/2$ phase lag between the x and y components in case of aligning the axis with respect to the semi-major and semi-minor axes of the projection of the current locus in the voltage plane. Moreover, this selection of reference frame simplifies notably the computation of the power terms $p(t)$, P and Q. These power terms are formulated as a function of the current locus (I_x and ϵ_i) and the balance voltage (V_x). This is not the case for the instantaneous reactive power $q(t)$ which involves the use of the o current component. On the contrary than in the balanced load case, the instantaneous reactive power is a periodic non-linear function with an average which is not related to the total reactive power Q.

REFERENCES

[1] T. Gozel and L. F. Ochoa, *Deliverable 3.3 '(Updated) Performance Evaluation of the Monitored LV Networks'*. U.K.: Electricity North West Limited, Jul. 2014. [Online]. Available: https://research.manchester.ac.uk/en/publications/deliverable-33-updated-performance-evaluation-of-the-monitored-lv, doi: 10.13140/RG.2.1.2773.1926.

[2] Y. Peng, Z. Shuai, J. M. Guerrero, Y. Li, A. Luo, and Z. J. Shen, "Performance improvement of the unbalanced voltage compensation in islanded microgrid based on small-signal analysis," *IEEE Trans. Ind. Electron.*, vol. 67, no. 7, pp. 5531–5542, Jul. 2020.

[3] L. Meng, X. Zhao, F. Tang, M. Savaghebi, T. Dragicevic, J. C. Vasquez, and J. M. Guerrero, "Distributed voltage unbalance compensation in islanded microgrids by using a dynamic consensus algorithm," *IEEE Trans. Power Electron.*, vol. 31, no. 1, pp. 827–838, Jan. 2016.

[4] M. Barragan-Villarejo, J. M. Mauricio, J. C. Olives-Camps, F. J. Matas-Diaz, F. D. P. Garcia-Lopez, and J. M. Maza-Ortega, "Harmonic and imbalance compensation in grid-forming VSC," in *Proc. IEEE Int. Conf. Ind. Technol. (ICIT)*, Feb. 2020, pp. 757–762.

[5] W. C. Duesterhoeft, M. W. Schulz, and E. Clarke, "Determination of instantaneous currents and voltages by means of alpha, beta, and zero components," *Trans. Amer. Inst. Electr. Eng.*, vol. 70, no. 2, pp. 1248–1255, 1951.

[6] R. H. Park, "Two-reaction theory of synchronous machines: Generalized method of analysis—Part I," *Trans. Amer. Inst. Electr. Engineers*, vol. 48, no. 3, pp. 716–727, Jul. 1929.

[7] H. Akagi, Y. Kanazawa, and A. Nabae, "Instantaneous reactive power compensators comprising switching devices without energy storage components," *IEEE Trans. Ind. Appl.*, vol. IA-20, no. 3, pp. 625–630, May 1984.

[8] A. Ferrero and G. Superti-Furga, "A new approach to the definition of power components in three-phase systems under nonsinusoidal conditions," *IEEE Trans. Instrum. Meas.*, vol. 40, no. 3, pp. 568–577, Jun. 1991.

[9] V. Choqueuse, P. Granjon, A. Belouchrani, F. Auger, and M. Benbouzid, "Monitoring of three-phase signals based on singular-value decomposition," *IEEE Trans. Smart Grid*, vol. 10, no. 6, pp. 6156–6166, Nov. 2019.

[10] P. Granjon and G. S. L. Phua, "Estimation of geometric properties of three-component signals for system monitoring," *Mech. Syst. Signal Process.*, vol. 97, pp. 95–111, Dec. 2017, doi: 10.1016/j.ymssp.2017.04.002.

[11] F. Milano, G. Tzounas, I. Dassios, and T. Kerci, "Applications of the FreNet frame to electric circuits," *IEEE Trans. Circuits Syst. I, Reg. Papers*, vol. 69, no. 4, pp. 1668–1680, Apr. 2022.

[12] P. Salmeron-Revuelta, "Análisis y simulación de las componentes instantáneas de intensidad en sistemas polifásicos con cargas no lineales y tensiones no senoidales," Ph.D. dissertation, Dept. Elect. Eng., Univ. Seville, Seville, Spain, Univ. Seville, 1993. [Online]. Available: https://idus.us.es/xmlui/handle/11441/73240?locale-attribute=en

[13] F. G. Montoya and A. H. Eid, "Formulating the geometric foundation of clarke, park, and FBD transformations by means of Clifford's geometric algebra," *Math. Methods Appl. Sci.*, vol. 45, no. 8, pp. 4252–4277, May 2022.

[14] F. Milano, "A geometrical interpretation of frequency," *IEEE Trans. Power Syst.*, vol. 37, no. 1, pp. 816–819, Jan. 2022.

[15] A. H. Eid and F. G. Montoya, "A systematic and comprehensive geometric framework for multiphase power systems analysis and computing in time domain," *IEEE Access*, vol. 10, pp. 132725–132741, 2022. [Online]. Available: https://ieeexplore.ieee.org/document/9992202/

[16] F. G. Montoya, X. Prado, F. M. Arrabal-Campos, A. Alcayde, and J. Mira, "New mathematical model based on geometric algebra for physical power flow in theoretical two-dimensional multi-phase power circuits," *Sci. Rep.*, vol. 13, no. 1, pp. 1–14, Jan. 2023. [Online]. Available: https://www.nature.com/articles/s41598-023-28052-x

[17] A. A. Montanari and A. M. Gole, "Enhanced instantaneous power theory for control of grid connected voltage sourced converters under unbalanced conditions," *IEEE Trans. Power Electron.*, vol. 32, no. 8, pp. 6652–6660, Aug. 2017. [Online]. Available: https://ieeexplore.ieee.org/abstract/document/7740053

[18] G. Tan, J. Cheng, and X. Sun, "Tan-sun coordinate transformation system theory and applications for three-phase unbalanced power systems," *IEEE Trans. Power Electron.*, vol. 32, no. 9, pp. 7352–7380, Sep. 2017. [Online]. Available: http://ieeexplore.ieee.org/document/7676330/

[19] G. Tan, Z. Chen, Y. Zhang, J. Wei, X. Zeng, and X. Sun, "Three-dimensional coordinate transformation theory for three-phase four-wire unbalanced power electronic system," in *Proc. IEEE 4th Int. Electr. Energy Conf. (CIEEC)*, May 2021, pp. 1–6.

[20] G. Tan, J. Wei, W. Zhao, L. Qi, and X. Sun, "Application of three-dimensional unbalanced coordinate transformation to stand-alone four-leg voltage-source inverter," *IEEE Trans. Power Electron.*, vol. 37, no. 10, pp. 11686–11703, Oct. 2022, doi: 10.1109/TPEL.2022.3173396.

[21] G. Tan, Z. Chen, W. Zhao, and X. Sun, "Research on phase-locked loop technique based on three-dimensional coordinate transformation," *Eng. Res. Exp.*, vol. 4, no. 1, Feb. 2022, Art. no. 015013. [Online]. Available: https://iopscience.iop.org/article/10.1088/2631-8695/ac4de5

[22] F. Casado-Machado, J. L. Martinez-Ramos, M. Barragan-Villarejo, J. M. Maza-Ortega, and J. A. Rosendo-Macias, "Reduced reference frame transform: Deconstructing three-phase four-wire systems," *IEEE Access*, vol. 8, pp. 143021–143032, 2020.

[23] D. Bellan, "Analytical investigation of the properties of transients in unbalanced three-phase four-wire networks," *Energies*, vol. 15, no. 23, p. 9122, Dec. 2022. [Online]. Available: https://www.mdpi.com/1996-1073/15/23/9122/htm

[24] R. Mohanty, N. K. Sahu, and A. K. Pradhan, "Time-domain techniques for line protection using three-dimensional Cartesian coordinates," *IEEE Trans. Power Del.*, vol. 37, no. 5, pp. 3740–3751, Oct. 2022.

[25] C. J. O'Rourke, M. M. Qasim, M. R. Overlin, and J. L. Kirtley, "A geometric interpretation of reference frames and transformations: Dq0, clarke, and park," *IEEE Trans. Energy Convers.*, vol. 34, no. 4, pp. 2070–2083, Dec. 2019.

[26] T. A. Lipo, "A Cartesian vector approach to reference frame theory of AC machines," in *Proc. Int. Conf. Electr. Mach.*, 1984, pp. 1–4.

[27] F. Z. Peng and J.-S. Lai, "Generalized instantaneous reactive power theory for three-phase power systems," *IEEE Trans. Instrum. Meas.*, vol. 45, no. 1, pp. 293–297, Feb. 1996.

[28] C. L. Fortescue, "Method of symmetrical co-ordinates applied to the solution of polyphase networks," *Trans. Amer. Inst. Electr. Eng.*, vol. 37, no. 2, pp. 1027–1140, Jul. 1918.

[29] G. Chicco and A. Mazza, "100 years of symmetrical components," *Energies*, vol. 12, no. 3, p. 450, Jan. 2019. [Online]. Available: http://www.mdpi.com/1996-1073/12/3/450

FRANCISCO CASADO-MACHADO was born in Seville, Spain, in 1990. He received the degree in mechanical engineering, the degree in electrical engineering, and the M.Sc. degree in electric energy systems from the University of Seville, in 2014, 2015, and 2018, respectively, where he is currently pursuing the Ph.D. degree. He was with Abengoa, Seville, as a Power System Engineer, from 2014 to 2018. Since 2018, he has been with the Department of Electrical Engineering, University of Seville, as a Research Assistant. His research interests include power system modeling, analysis, and control.

JOSÉ L. MARTÍNEZ-RAMOS (Senior Member, IEEE) was born in Dos Hermanas, Spain, in 1964. He received the Ph.D. degree in electrical engineering from the University of Seville, Seville, Spain, in 1994. Since 1990, he has been with the Department of Electrical Engineering, University of Seville, where he is currently a Full Professor. His research interests include active and reactive power optimization, power system planning, analysis and control, and electricity markets.

MANUEL BARRAGÁN-VILLAREJO was born in Marmolejo, Spain, in 1984. He received the degree in electrical engineering and the Ph.D. degree in electrical engineering from the University of Seville, Seville, Spain, in 2008 and 2014, respectively. Since 2008, he has been with the Department of Electrical Engineering, University of Seville, where he is currently an Associate Professor. His primary research interests include the exploitation and control of power converters for smart grid management and the grid integration of renewable energy resources.

JOSÉ MARÍA MAZA-ORTEGA (Member, IEEE) received the degree in electrical engineering and the Ph.D. degree from the University of Seville, Spain, in 1996 and 2001, respectively. Since 1997, he has been with the Department of Electrical Engineering, University of Seville, where he is currently an Associate Professor. His research interests include power quality, harmonic filters, the integration of renewable energy, and power electronics.